

© Copyright 15 Nov 2009 American Meteorological Society (AMS). For permission to reuse any portion of this work, please contact permissions@ametsoc.org. Any use of material in this work that is determined to be “fair use” under Section 107 of the U.S. Copyright Act (17 U.S. Code §107) or that satisfies the conditions specified in Section 108 of the U.S. Copyright Act (17 USC § 108) does not require the AMS’s permission. Republication, systematic reproduction, posting in electronic form, such as on a website or in a searchable database, or other uses of this material, except as exempted by the above statement, requires written permission or a license from the AMS. All AMS journals and monograph publications are registered with the Copyright Clearance Center (<https://www.copyright.com>). Additional details are provided in the AMS Copyright Policy statement, available on the AMS website (<https://www.ametsoc.org/PUBSCopyrightPolicy>).

Access to this work was provided by the University of Maryland, Baltimore County (UMBC) ScholarWorks@UMBC digital repository on the Maryland Shared Open Access (MD-SOAR) platform.

Please provide feedback

Please support the ScholarWorks@UMBC repository by emailing scholarworks-group@umbc.edu and telling us what having access to this work means to you and why it’s important to you. Thank you.

The Influence of Solar Forcing on Tropical Circulation

JAE N. LEE

*School of Marine and Atmospheric Science, Stony Brook University, Stony Brook, New York, and
Jet Propulsion Laboratory, California Institute of Technology, Pasadena, California*

DREW T. SHINDELL

*NASA Goddard Institute for Space Studies, and Center for Climate Systems Research,
Columbia University, New York, New York*

SULTAN HAMEED

School of Marine and Atmospheric Science, Stony Brook University, Stony Brook, New York

(Manuscript received 9 June 2008, in final form 2 June 2009)

ABSTRACT

The response of the seasonal tropical circulation to an 11-yr solar cycle forcing is studied with the Goddard Institute for Space Studies (GISS) ModelE, which includes fully interactive atmospheric chemistry. To identify characteristic solar signals in the tropical circulation, the model experiments are carried out with certain imposed conditions: a doubly amplified solar forcing and the present-day and preindustrial greenhouse gases and aerosol conditions, with the mixed layer or fully coupled dynamic ocean model. In both the model and the NCEP reanalysis, tropical humidity increases in response to enhanced solar irradiance are found to be statistically significant in both solstice seasons. Changes are also found in the vertical velocities for both the Hadley and Walker circulations in some areas of the Pacific region. With present-day greenhouse gas and aerosol conditions, the ascending branch of the Hadley cell is enhanced near the equator, and the intertropical convergence zone (ITCZ) is shifted northward in response to solar forcing during the boreal winter. Enhancement of the meridionally averaged vertical velocity over the western Pacific indicates strengthening of the Walker circulation in response to solar forcing in both solstice seasons. In present-day conditions, the tropical circulation response to an 11-yr solar forcing is generally consistent with that derived from previous observational works.

1. Introduction

The hypothesis by van Loon and Labitzke (1994) that vertical motion in the tropics is correlated with the decadal solar oscillation has been supported by observational evidences (e.g., Gleisner and Thejll 2003; Salby and Callaghan 2005; Kodera 2004). Some of the observational studies suggest that the thermal solar signal is preferentially strong in subtropical Pacific areas and affects the moisture transport and precipitation in these regions (van Loon et al. 2004, 2007). Kodera and Shibata (2006) suggest that Indian Ocean monsoon circulation is

correlated with 11-yr solar cycle via altered planetary wave fraction and stratospheric meridional circulation changes.

Paleoclimate lake and marine records indicate changes on longer time scales in the regional hydrological cycle during the Holocene (to ~10 kyr BP), even though discrepancies exist between them about the timing and nature of the changes. The dominant forcing for the Holocene is known to be the seasonal contrast of incoming solar radiation at the top of the atmosphere (Berger 1978). This solar forcing is an important factor for regional changes in monsoon, vegetation, and lake levels, which can then influence the global hydrological and energy cycles. Analysis of the lake sediment records suggest that the historically severe droughts in the Yucatan peninsula during the period 800–1000 AD might have occurred during times of increased solar output

Corresponding author address: Jae N. Lee, Jet Propulsion Laboratory, California Institute of Technology, M/S 169-237, 4800 Oak Grove Dr., Pasadena, CA 91109.
E-mail: jae.nyung.lee@jpl.nasa.gov

(Hodell et al. 2001). Conversely, the Ti content data from the Cariaco Basin ($\sim 10^\circ\text{N}$) ocean sediment (Haug et al. 2003) suggests wetter conditions in northern South America with increased solar insolation. The *Globigerina bulloides* $\delta^{18}\text{O}$ record of the Cariaco Basin also shows wetter or warmer conditions when sunspot numbers are high (Black et al. 2004). Because this location is farther south, this record contrasts with the dry conditions inferred from the lake records of the Yucatan. The $\delta^{18}\text{O}$ values of stalagmite from southern Oman suggest that monsoon precipitation decreased gradually in response to declining Northern Hemisphere summer solar insolation during the middle-to-late Holocene (Fleitmann et al. 2003). Annual Nile records of the water level for 622–1470 AD is found to be linked to the 88- and 208-yr solar variability (Ruzmaikin et al. 2006). It is also reported that the Florida Strait was in drier conditions with anomalously high surface salinities during the Little Ice Age (Lund et al. 2006). Serious cooling period of the Little Ice Age (1645–1745 AD) is believed to be associated with the late seventeenth century low solar irradiance event, the Maunder Minimum. Paleoclimate records also show a link between centennial-scale southward migrations of the Atlantic intertropical convergence zone (ITCZ) and declining Northern Hemisphere summer solar insolation by orbital forcing (Haug et al. 2001). Hence, there is a substantial body of evidence indicating that solar forcing affects the tropical hydrologic cycle.

In addition to these observational and proxy studies, there are many climate modeling efforts (e.g., Shindell et al. 2001; Schmidt et al. 2004; Rind et al. 2005; Otto-Bliesner et al. 2006; Carlson et al. 2008) that access the nature and amplitude of the paleoclimate change resulting from solar forcing. There are also successful modeling studies of the present-day (PD) climate (Meehl et al. 2003; Meehl and Hu 2006; Matthes et al. 2006; Shindell et al. 2006a; Rind et al. 2008) that further investigate the dynamic couplings and feedbacks of the tropical circulation resulting from solar forcing.

Solar radiation changes at UV wavelengths are primarily absorbed in the stratosphere, where a clear signal of heating in solar maximum versus solar minimum is seen in observations (e.g., Kodera 2004; Salby and Callaghan 2005; Kodera and Shibata 2006). Solar radiation changes at longer wavelengths, which are less than those in the UV in terms of percent change (Lean 2000) but nonetheless include most of the total flux change, clearly reach the earth's surface and affect surface temperature. Model results to date indicate that variations in UV flux absorbed in the stratosphere have only a minimal impact on global mean surface temperatures [a slight enhancement to the response to total solar irradiance (TSI)]. However, the UV flux changes appear

to be able to induce substantial changes in circulation, with distinct regional climate effects (Kodera 2004; Shindell et al. 2006b; Matthes et al. 2006). Regional responses to solar forcing may also occur in response to the TSI component, which will have an inhomogeneous effect on the surface because of nonuniform cloud coverage leading to circulation changes (Meehl et al. 2003). Both sets of circulation changes may be operating simultaneously. However, it is difficult to distinguish the solar UV effect from that of TSI, because to date the modeling works force the entire spectrum of solar variability in one simulation.

Meehl et al. (2003) suggest a mechanism in which the enhanced solar forcing produces greater evaporation and moisture in the precipitation convergence zones, a more intensified regional monsoon, and strengthened Hadley and Walker circulations that cause cloud reductions, and hence lead to a configuration where more solar input reaches the subtropical ocean region. Thus, the sensitivity of the tropical circulation response can cause the solar forcing to be amplified in the cloud-free subtropics through positive feedbacks. Matthes et al. (2006) show that the vertical velocity response is most significant over the Indian Ocean and western Pacific with the Freie Universität Berlin Climate Middle Atmosphere Model (FUB-CMAM). Shindell et al. (2006a) also show that the persistent solar forcing induces increased precipitation in the tropical western Pacific region from a simulation with a dynamic ocean coupled to the Goddard Institute for Space Studies (GISS) ModelE general circulation model (GCM). Rind et al. (2008) show an increased stratospheric residual circulation response from the Southern to Northern Hemispheres to solar forcing and the poleward extension of the Hadley circulation with a vast number of GISS Global Climate Middle Atmosphere Model 3 simulations.

In the present paper, using the GISS ModelE chemistry and coupled atmosphere–ocean GCM, the model experiments are designed to investigate the role of 11-yr cycle solar forcing on seasonal tropical circulation. A doubly amplified solar forcing and different anthropogenic forcings are imposed on models with different ocean modules. Amplified solar variability is used to enhance the signal-to-noise ratio. Comparison of the simulations with different amplitudes of solar forcing also permits us to observe the linearity of the climate response to solar variability. Two different atmospheric compositions are imposed: one with PD greenhouse gases and aerosol conditions and the other with the preindustrial (PI) conditions.

From each simulation, the statistically significant solar signals in the tropospheric specific humidity are presented for January and July. We also show solar signals

TABLE 1. Description for each GISS ModelE solar forcing simulation. Each simulation is conducted for perpetual solar maximum and minimum conditions, respectively. The term ΔS is half of the 1.1 W m^{-2} solar irradiance change.

Simulations	Solar forcing	Composition	Ocean	Length (yr)
PD (PD-qflux)	$+\Delta S \sim -\Delta S$	PD	<i>q</i> -flux	37
PI (PI-qflux)	$+\Delta S \sim -\Delta S$	PI	<i>q</i> -flux	37
Double forcing (DF-PD-qflux)	$+\Delta S \sim -2 \times \Delta S$	PD	<i>q</i> -flux	37
Dynamic coupled ocean model (PI-HYCOM)	$+\Delta S \sim -\Delta S$	PI	HYCOM	60

in the vertical velocity in each simulation over the Pacific region, where the zonally asymmetric response pattern plays an important role in the tropical circulation.

2. Model experiments

Four model simulations are performed separately for two solar activity conditions: solar maximum and solar minimum. Each pair of simulations, except the double minimum run, is forced with 11-yr irradiance changes that take place over the solar cycle for perpetual solar maximum (MAX) and perpetual solar minimum (MIN) conditions. The 11-yr solar cycle irradiance change corresponds to $\sim 0.19 \text{ W m}^{-2}$ instantaneous radiative forcing at the tropopause, which is equivalent to 1.1 W m^{-2} in solar irradiance change at the top of the atmosphere. For the double minimum run, the amplitude of the solar cycle change is doubled to enhance the tropical circulation response. The spectrally varying solar irradiance perturbation input to the three-dimensional chemistry coupled atmospheric model produces stratospheric and tropospheric ozone changes (Shindell et al. 2006b). GISS ModelE produces maximum ozone change in the mid-stratosphere with solar forcing, whereas in the observations there are double ozone response peaks in the upper and lower stratosphere in solar maximum condition (Soukharev and Hood 2006).

Four pairs of model experiments are carried out to investigate the role of solar forcing in the tropical circulation: one with the PD greenhouse gases and aerosol conditions and a mixed-layer (*q*-flux) ocean (PD-qflux), one with the PI conditions (PI-qflux), one with doubled minimum solar forcing (DF-PD-qflux), and one with the PI conditions and with the Hybrid-Coordinate Oceanographic Model (HYCOM; PI-HYCOM; Table 1). For the preindustrial cases, all anthropogenic emissions into the troposphere are removed, and long-lived greenhouse gases are set to the conditions at 1850. Biomass burning emissions were set to 10% of their PD values. The *q*-flux ocean model is a simplified thermodynamic mixed-layer ocean model, where the SST is allowed to adjust to different atmospheric fluxes but the ocean heat transport is held constant (Schmidt et al. 2006). The oceanic heat convergence (*q*-fluxes) into the isothermal

mixed layer is calculated as a residual given by the heat and mass fluxes at the base of the atmosphere. The HYCOM includes 16 isopycnal vertical layers with a horizontal resolution of $2^\circ \times 2^\circ$ cos(latitude), and produces a relatively reasonable magnitude of El Niño–Southern Oscillation (ENSO)-like variability (Sun and Bleck 2006). The PI runs are targeted to estimate the most pronounced long-term recent solar minimum event, the Maunder Minimum, when the sun's output was reduced and only a few sun spots appeared. The reduction in irradiance at that time is thought to be approximately equal to the difference between solar maximum and minimum of the 11-yr solar cycle (Wang et al. 2005).

The PD and the PI model experiments are plotted to see whether greenhouse gas increase can make an influence on tropical circulation response to solar variability. Comparing these two model experiments, the PD-qflux and the PI-qflux represent a possible shift of responses to identical solar forcing with two different present-day and preindustrial greenhouse gases and aerosol conditions. Comparisons between the PI-qflux and the PI-HYCOM show a possible difference of responses to identical solar forcing between mixed-layer (*q*-flux) ocean and fully coupled ocean (HYCOM) models. The 23-layer version of ModelE resolves the stratosphere, extending from the surface to 0.02 hPa, and includes a parameterization of the gravity wave drag. The model output is given on a 4° latitude \times 5° longitude grid. Further details on the model are given in Schmidt et al. (2006). According to Rind et al. (2008), finer horizontal and vertical resolutions ($2^\circ \times 2.5^\circ$ and $4^\circ \times 5^\circ$, with 23, 53, and 102 layers) do not produce a stronger tropospheric response to solar forcing in their simulation experiments with the GISS Global Climate Middle Atmosphere Model 3.

The responses of the model to solar forcing are presented as differences between MAX and MIN simulations. In a previous analysis, using the identical model output, the index for the northern annular mode (NAM) in the stratosphere was found to stabilize after the first 20 yr of simulation (Lee et al. 2008). For this reason, the analysis presented in this paper is for the last 17 yr from the 37 yr of both MAX and MIN runs that are coupled to the *q*-flux ocean module. For the

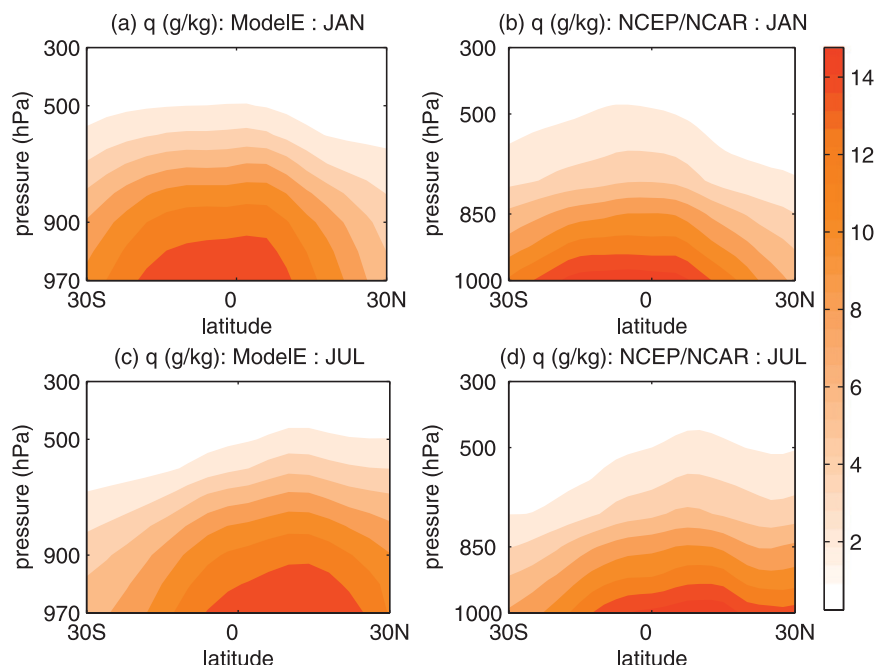


FIG. 1. Zonally averaged specific humidity (g kg^{-1}) in January for (a) the model PD-qflux simulation and (b) the NCEP-NCAR reanalysis and in July for (c) the model PD-qflux simulation and (d) the NCEP-NCAR reanalysis.

PI-HYCOM simulation, the last 30 yr of the 60 yr of the run are analyzed.

3. Solar signal in specific humidity

a. Local specific humidity

Midtropospheric humidity is highest in the convective region between 20°S and 10°N in January and between 10°S and 20°N in July, as the convective region moves toward the respective summer hemisphere (Fig. 1). The climatology of zonally averaged specific humidity is shown for the model (Figs. 1a,c) and for the National Centers for Environmental Prediction–National Center for Atmospheric Research (NCEP–NCAR) reanalysis (Kalnay et al. 1996; Figs. 1b,d). Uncertainties in solar signal from the reanalysis are caused by other greater forcing factors, such as ENSO, volcanic eruptions, and anthropogenic increase of the humidity (Gleisner and Thejll 2003).

Midtropospheric humidity decreases sharply with latitude both in the model and in the NCEP–NCAR reanalysis. This latitudinal distribution of specific humidity does not result from the temperature variations but from the descending branch of the Hadley cell (Pierrehumbert 2001). The air in the subsiding branch is dry, because it is brought down from a cold and dry place with conserved specific humidity. Although the subsidence region is dry

compared to the ITCZ, it is still humid because of the latitudinal transport of moisture by turbulent eddies (Pierrehumbert et al. 2005). Tropospheric humidity also decreases with altitude both in the model and in the reanalysis. However, the humidity in the GISS model decreases more slowly with altitude and shows more humidity in the troposphere compared to the reanalysis. A comparison of the atmospheric infrared sounding (AIRS) and reanalysis specific humidity profiles with the 16 different modeling works presented by John and Soden (2007) shows that other models also simulate more column-integrated humidity than in observations. Increases of humidity in models contribute to greenhouse effect by emitting longwave radiation toward the surface and warming the lower troposphere. Because the relative humidity is forced to stay constant in models, the troposphere gets more humidity with warm temperature biases (M. Khairoutdinov 2008, personal communication). However, the influence of solar forcing on the humidity response depends primarily on the difference of the humidity field, rather than on the mean state of model simulation. Thus, the impact of this humid bias on the sun–climate studies remains unclear.

In Figs. 2a–d and 3a–d, for January and July, respectively, the responses of specific humidity to solar forcing are calculated as the differences of zonal mean composites of specific humidity between the MAX and

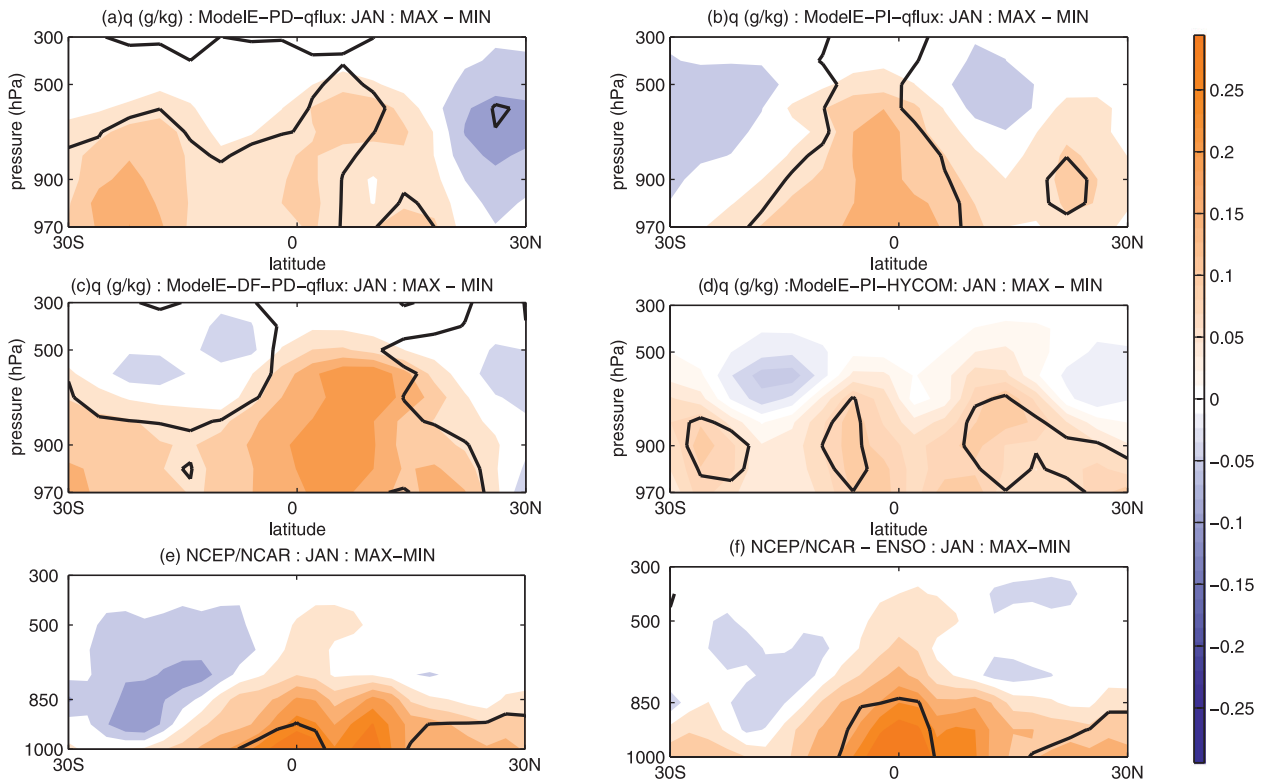


FIG. 2. Differences of the zonally averaged specific humidity (g kg^{-1}) between solar maximum and solar minimum in January for (a) the PD-qflux simulation, (b) the PI-qflux simulation, (c) the DF-PD-qflux (double minimum forcing) simulation, (d) the PI-HYCOM simulation, (e) the NCEP-NCAR reanalysis with all years, and (f) the NCEP-NCAR reanalysis with non-ENSO years. The solid lines represent 95% significant level of Student's t test.

MIN simulations. The corresponding differences obtained from the NCEP-NCAR reanalysis with all years and with non-ENSO years are shown in Figs. 2e,f and 3e,f for January and July, respectively. For the reanalysis, the 11-yr solar cycle is quantified by the 200–295-nm solar UV flux from Lean (2000). For the period from 1948 to 2004, the months with monthly mean UV above (below) one standard deviation from the mean are grouped as solar maximum (minimum): 10 (12) months for July and 10 (11) months for January. Solar maximum and minimum months are nearly identical with the above conditions (9 and 11 months for July and 8 and 10 months for January, respectively) when solar maximum and minimum conditions are classified with solar 10.7-cm radio flux. The extreme positive and negative ENSO years (1965, 1975, and 1997 for July; 1958, 1976, 1987, and 1989 for January) were filtered out from MAX or MIN years for the non-ENSO composites. Both the model and the reanalysis consistently show that the specific humidity is greater in the convective region in solar maximum compared to minimum for both seasons. The lowest level of the atmosphere seems to be moistened by solar forcing over the oceanic regions.

In January, the humidity changes in the PD-qflux and DF-PD-qflux (doubled minimum forcing) simulations (Figs. 2a,c) show similar broad moistening of the tropics in 30°S – 20°N , but the response is enhanced by the amplified forcing in the DF-PD-qflux simulation. Responses from the PI-qflux (Fig. 2b) and the PI-HYCOM (Fig. 2d) simulations are consistent for the two significant response regions: one near the equator and the other in the north of the strong convection region. The PI-qflux run appears to show a stronger equatorial response than the PD-qflux run. In the PI-HYCOM, humidity response has a different structure than in the other experiments and in the NCEP-NCAR reanalysis, but significant response is in lower troposphere, as in the reanalysis. The most significant humidity differences between solar maximum and solar minimum in the NCEP-NCAR reanalysis (Figs. 2e,f) are shown at the lowest tropospheric level. The statistically significant solar signal is extended to 850 hPa near the equator by filtering out strong ENSO years. Solar signals in the specific humidity show consistent moistening of the tropics in the model as well as in the reanalysis. However, solar signals are statistically significant throughout the troposphere, including the southern

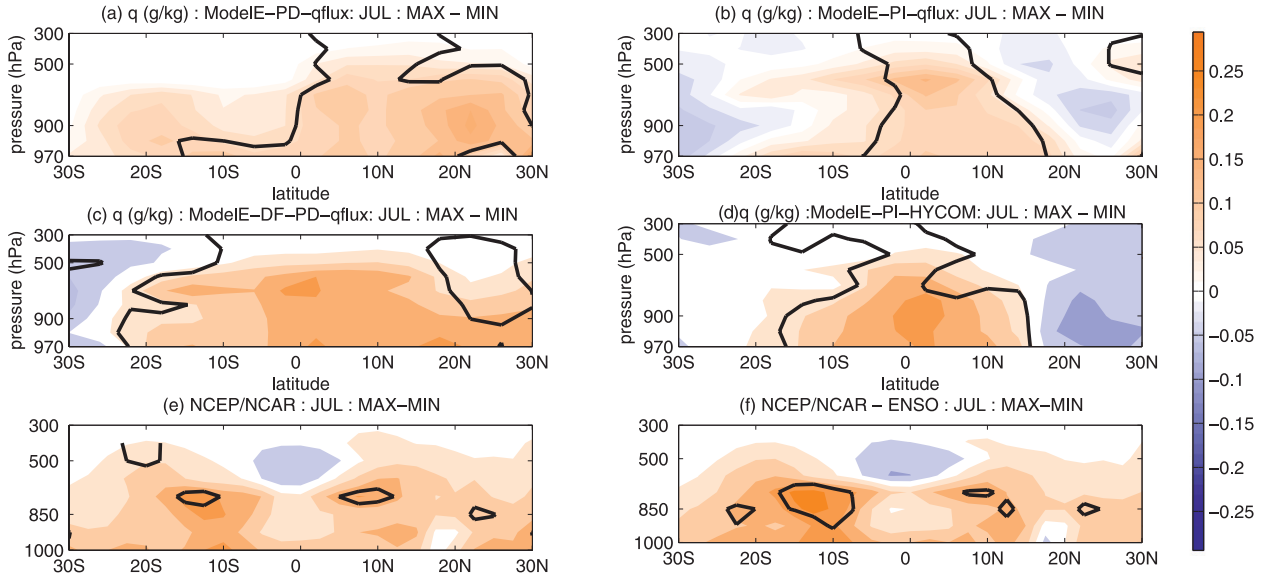


FIG. 3. As in Fig. 2, but for July.

subtropics, in the model, whereas the significant solar signal is limited to the lower troposphere and does not extend into the Southern Hemisphere subtropics in the reanalysis, especially during January. It has been already shown that the variability of the upper-level humidity is highly correlated to the surface humidity in models, whereas the upper-level humidity quickly decorrelates in observations (Sun and Held 1996). This reflects the fact that the anomalies of the humidity in models are strongly forced by those of the adjacent levels. The greater variability of the data in the reanalysis caused by other forcing factors, such as ENSO, volcanic eruptions, and anthropogenic increase of the humidity (Gleisner and Thejll 2003), is partly responsible for the areas of statistical significance in the reanalysis being smaller than those in the model. Fewer degrees of freedom limited by short periods of observation from the reanalysis compared to those from the model can also contribute to this difference. By considering the autocorrelation of the each sample, the effective degrees of freedom are estimated as ~ 10 for N_{NCEP} and ~ 21 for N_{MODEL} by Quenouille's procedure, as described by Angell and Korshover (1981). A good estimate of the effective number of independent observations is given by

$$\frac{N}{(1 + 2r_1r'_1 + 2r_2r'_2 + \dots)}, \quad (1)$$

where N is the number of data points in each of the two series, r_1 and r'_1 are the lag-one autocorrelations of the two series, r_2 and r'_2 are the lag-two autocorrelation of the two series, etc. These effective numbers are applied to determine the significance with Student's t test.

In July, humidity changes in the PD-qflux simulation (Fig. 3a) show broad moistening over 30°S – 30°N . Specific humidity change in the DF-PD-qflux simulation (Fig. 3c) is consistent with the PD-qflux simulation, but the response is enhanced by the amplified forcing. The latitude band of the significant positive signal is narrowed toward the equator under the preindustrial greenhouse gas and aerosol conditions in the PI-qflux and PI-HYCOM simulations compared to the PD-qflux and DF-PD-qflux cases. Such responses lead to a stronger humidity gradient in the north of the convective region during solar maximum. Humidity response in the PI-HYCOM is amplified during July relative to the PI-qflux run. In the reanalysis (Figs. 3e–g), the most significant solar signals are shown around 10°N and 10°S , whereas those in the models are shown near the equator. The double maximum in the reanalysis is not present in either of the model experiments. Large variability of the summertime humidity, caused by monsoons, is considered to cause the broadened solar signal in the reanalysis. The reasons for other forcing factors, which are responsible for the difference between the reanalysis and the model, are considered to be similar to that discussed previously for January. Solar signals in the reanalysis are also extended to the midtroposphere in July, whereas they are confined within the low troposphere in January. The statistical significance of the solar signal in the reanalysis is vertically extended to ~ 700 hPa near 10°S by filtering out strong ENSO years.

During the solar maximum condition, the greater solar energy input to the tropical surface air is converted

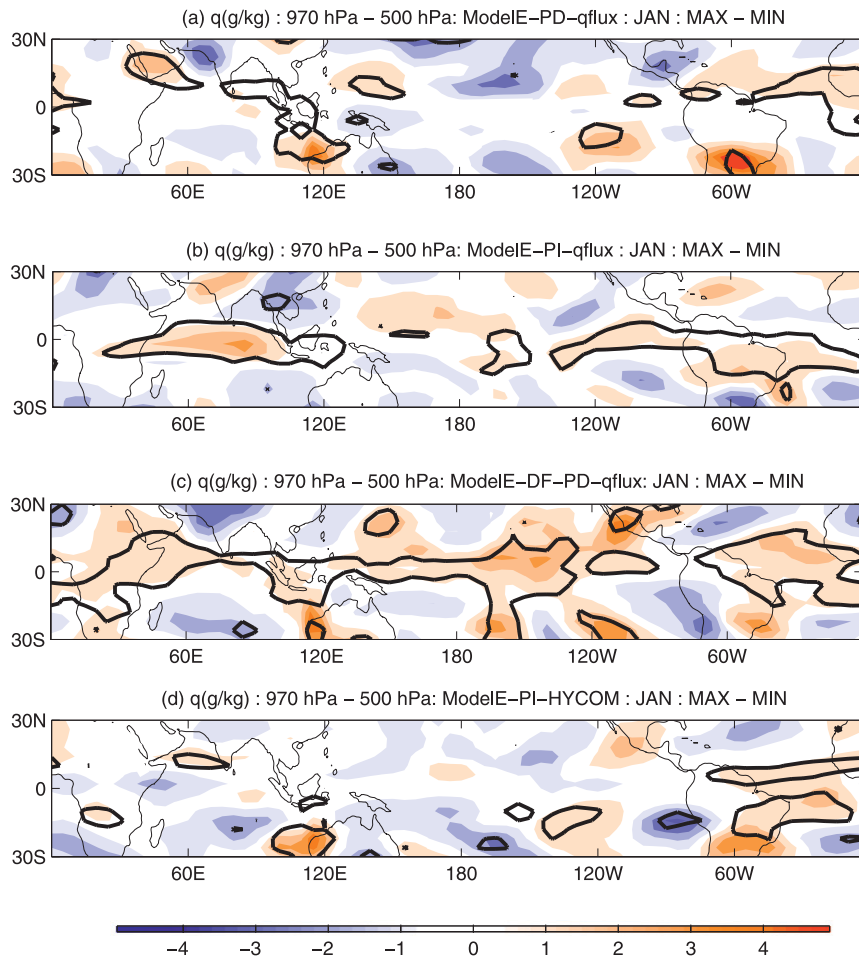


FIG. 4. Differences of integrated specific humidity (g Kg^{-1}) from 970 to 500 hPa in January for (a) the PD-qflux simulation, (b) the PI-qflux simulation, (c) the DF-PD-qflux (double minimum forcing) simulation, and (d) the PI-HYCOM simulation. The solid lines represent 95% significant level of Student's t test.

into higher SST through air–sea interaction (White et al. 2003) and into greater specific humidity in the boundary layer. The increase of the humidity provides more liquid water content in clouds and makes the precipitation process more efficient in the ascending regions of convective systems. However, efficient convective precipitation leaves less water vapor available for detrainment and reduces cirrus coverage, the precipitation, and the humidity in the northward part of the convective region (Lindzen et al. 2001). These responses of enhanced precipitation in the ascending branch and drying in the subtropics are also consistent with an earlier analysis of Shindell et al. (2006a) indicating increased precipitation near the equator and decreases at subtropical to middle latitudes and an enhanced Asian monsoon. This is also consistent with the theoretical response to global warming in general, as outlined in Held and Soden (2006). Similar to our seasonal responses, Gleisner and Thejll

(2003) also show moistening of the tropical troposphere during solar maximum by extracting the correlation between solar 10.7-cm radio flux and annual mean NCEP–NCAR reanalysis thickness after filtering out ENSO and volcanic signals.

b. Column-integrated specific humidity

The model-simulated specific humidity, integrated over 500–970 hPa, is high in the equatorial band with a substantial latitudinal gradient over the Pacific. The difference of the integrated specific humidity between MAX and MIN is shown for January and July in Figs. 4a–d and 5a–d, respectively. In the equatorial band, positive solar signals are found in the Atlantic sector in both seasons. In January, this positive signal in the PD-qflux run extends from the Amazon area to equatorial western Africa and to the western coast of Australia. In the PI-qflux run, the positive signal extends to the eastern

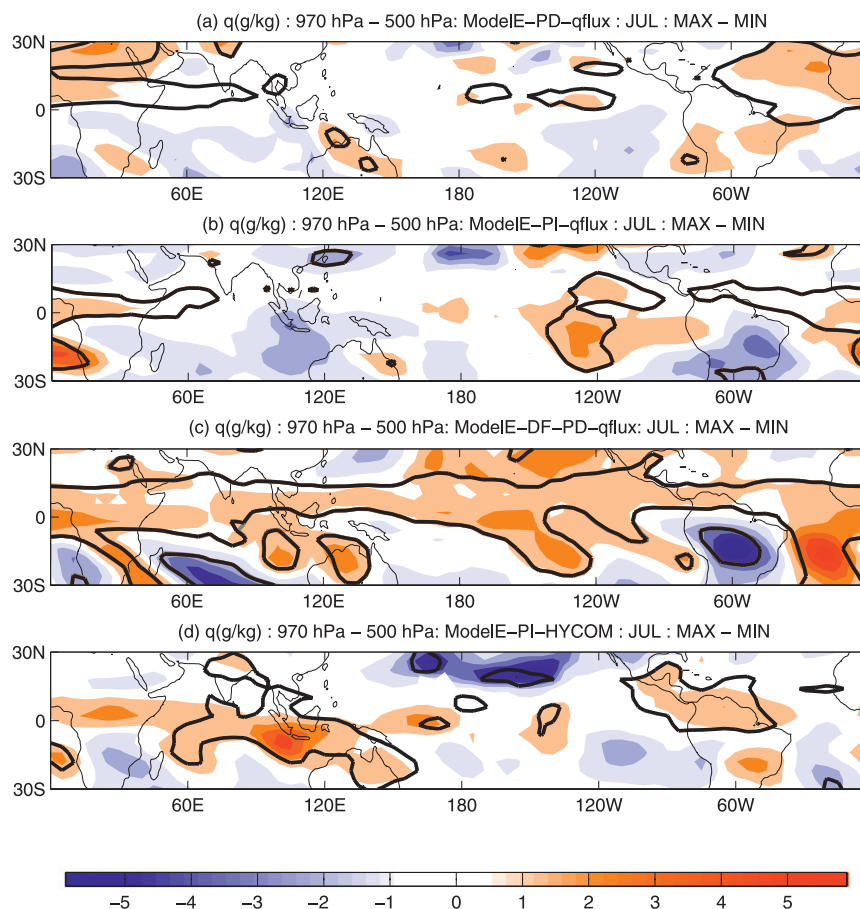


FIG. 5. As in Fig. 4, but for July.

Pacific and Indian Oceans. The positive humidity signal in the DF-PD-qflux run is significant throughout the equatorial band, including the Indonesian archipelago. In July, the positive solar signals in the PD-qflux run are more significant in the northern Atlantic sector and extend toward Africa and India. The PI-qflux run shows a positive center in the Indian Ocean and in the eastern Pacific. Similar to January, the positive signal in the DF-PD-qflux run is also significant throughout the equatorial band in July. The PI-HYCOM run suggests an intensified summer monsoon in Africa and India (Fig. 5d). These agree with the work of Meehl et al. (2003), demonstrating that enhanced solar forcing induces more evaporation over the moisture-divergent oceanic regions and that the increased moisture converges into the precipitation zones, intensifying the regional African and Indian monsoons.

The record in a stalagmite from Qunf Cave ($\sim 17^\circ\text{N}$) in southern Oman (Fleitmann et al. 2003) indicates the gradual long-term increase in Indian monsoon precipitation intensity during early Holocene (between 10.3 and 9.6 kyr BP) in response to increase of June–August

summer insolation. Lund et al. (2006) suggested a strong climate link between the Florida Strait and Cariaco Basin (Haug et al. 2003) that the Florida Strait was in drier conditions with anomalously high surface salinities during the Little Ice Age. Lake sediment core records from Yucatan Peninsula ($\sim 20^\circ\text{N}$) suggest a contrasting solar–precipitation relationship indicating that the century-scale evaporation/precipitation (E/P) ratio was enhanced with high solar activity over the past 2600 yr (Hodell et al. 2001). At this location, farther north of the Cariaco Basin, these records are consistent with the humidity response from the PI-HYCOM simulation.

The significant solar signals in the integrated tropospheric humidity (500–970 hPa) over the equator, especially in DF-PD-qflux run (Figs. 4c, 5c), coincide with the peak solar signals in the annual mean tropospheric thickness (500–1000 hPa) shown in Gleisner and Thejll (2003) with the NCEP–NCAR reanalysis. Geopotential thickness is defined as the height difference between two isobaric surfaces; it is linearly related to the mean temperature and the integrated humidity of the layer (Zhang et al. 2001). In the DF-PD-qflux simulation

(Fig. 5c), the positive solar signal over the Atlantic Ocean is located south of the equator. The contrasting hydrologic signals existing between the Atlantic coastal region and South America, as seen in Fig. 5c, agree well with similar patterns appearing in the paleoclimate records. Pollen records from the southern Amazonia have a negative correlation with the precipitation in the Cariaco Basin record (Mayle et al. 2000). Records of Brazil's wet periods obtained from speleothems and travertine deposits are also synchronous with the dry periods of decreased river runoff to the Cariaco Basin (Wang et al. 2004). Note that the simulations with the q -flux model appear more realistic in this respect than those with the HYCOM model.

c. Estimated radiative effect

Longwave net radiative flux difference between solar maximum and solar minimum periods is calculated to estimate the radiative effect resulting from the column-integrated specific humidity change induced by the solar forcing, as discussed in section 3b. Radiative effect due to humidity change is calculated by applying vertical profiles of zonally averaged specific humidity over 30°N from the NCEP–NCAR reanalysis for both the solar maximum and the solar minimum to the second version of the NCAR Community Climate Model (CCM2) clear-sky radiation parameterization scheme (Hack et al. 1993). Other parameters are fixed from the climatology. The United Kingdom Universities Global Atmospheric Modeling Program (UGAMP) ozone profile (Li and Shine 1995) is used for the ozone climatology. The longwave net flux at 30°N calculated from solar maximum is $\sim 0.2 \text{ W m}^{-2}$ greater than that from solar minimum at the tropopause. The maximum 2% integrated water vapor change in the NCEP reanalysis resulting from solar forcing is roughly equivalent to 10% of the estimated increase of the global mean column-integrated water vapor caused by 3 K temperature increase with doubling of CO_2 (Held and Soden 2006). The climate sensitivity parameter, the increase in global average surface temperature per W m^{-2} of radiative forcing, of the 23-layer GISS ModelE with the mixed-layer ocean model is 2.4 K with doubling of CO_2 , and this amount is equivalent to 0.6 K per W m^{-2} . For context, the Fourth Assessment Report (AR4) models have a range of 2–4.5 K temperature increase with doubling of CO_2 . As estimated by Held and Soden (2006) for coupled GCMs participating in Intergovernmental Panel on Climate Change (IPCC) AR4, the water vapor feedback is the strongest positive feedback, adding $1.80 \pm 0.18 \text{ W m}^{-2} \text{ K}^{-1}$, followed by the lapse rate ($-0.84 \pm 0.26 \text{ W m}^{-2} \text{ K}^{-1}$) and the cloud feedbacks ($0.69 \pm 0.38 \text{ W m}^{-2} \text{ K}^{-1}$; Bony et al. 2006).

4. Solar signal in tropical circulation

Meehl et al. (2003) suggested a feedback mechanism for solar forcing: enhanced irradiance produces greater evaporation, intensifying the regional monsoon and the Hadley and Walker circulations in the tropics, leading to cloud reductions and hence more solar input over the subtropical ocean regions. Van Loon et al. (2004), Kodera (2007), and van Loon et al. (2007) showed significant differences in the seasonal vertical velocity (ω) over the tropics between solar maximum and minimum that appear to be at least qualitatively consistent with this mechanism.

The tropical circulation responds to solar forcing by redistributing the zonally asymmetric diabatic heating. To further investigate the changes of the tropical Hadley and Walker circulations resulting from solar forcing, we show the differences in the zonally or meridionally averaged vertical motion ω between the MAX and MIN model outputs within the tropical Pacific region (Figs. 6–9). The solar signals in the tropical circulations are compared to those seen by van Loon et al. (2004, 2007) using NCEP–NCAR reanalysis.

a. Solar signal in tropical circulation in January

The model climatology of the zonally averaged vertical velocity ω in pressure coordinates during the month of January (Fig. 6a) shows the typical winter season features of vertical motion: that is, rising motion over the tropics from 20°S to 10°N, which peaks at 850 hPa, and strong sinking motion around 30°N, which peaks at 500 hPa. Despite the uncertainties of vertical velocity in models, a comparison of GISS ModelE, Tropical Rainfall Measuring Mission (TRMM) convective–stratiform heating (CSH) product, and the reanalysis (Chen et al. 2007) shows that the model vertical velocity is comparable to that in the reanalysis over the tropical Maritime Continent. However, over the tropical Pacific region, downward motion between the two upward rising bands is shifted west in the model climatology (Fig. 7a) compared to those shown in van Loon et al. (2007) with the NCEP–NCAR reanalysis.

Statistically significant differences of vertical velocity between MAX and MIN in the PD- q -flux simulation (Fig. 6b) suggest that the ascending motion in the Hadley cell is enhanced north and south of the equator throughout the troposphere in the solar MAX run. The DF-PD- q -flux simulation (Fig. 6d) shows similar solar signal as the PD- q -flux simulation, but with more weakening of the descending branch. The changes in the vertical motion are not significantly increased by doubling the solar forcing. These signals in the PD- q -flux and DF-PD- q -flux simulations indicate that the ascending

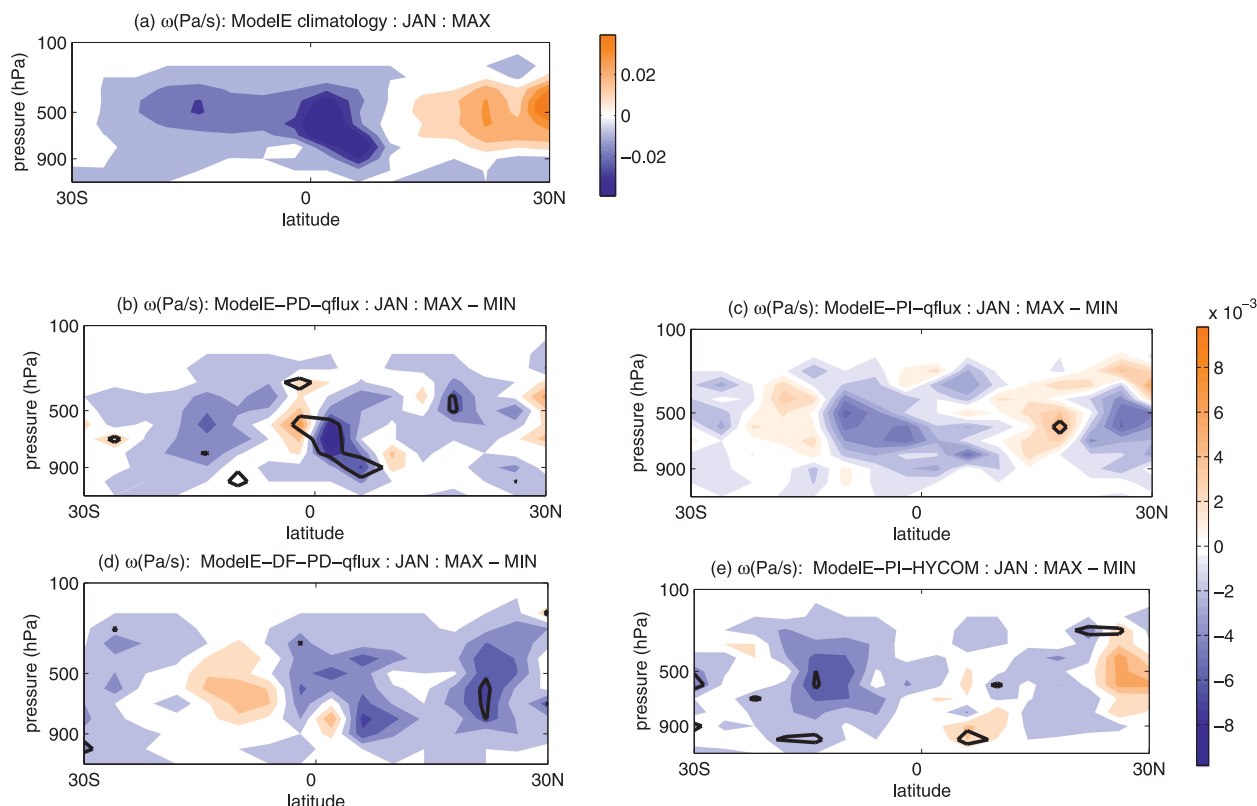


FIG. 6. Zonally averaged vertical velocity ω over the tropical Pacific (150°E – 100°W) during the month of January in Pa s^{-1} for (a) the climatology from the model simulation, as well as the difference between MAX and MIN for (b) the PD-qflux simulation, (c) the PI-qflux simulation, (d) the DF-PD-qflux simulation, and (e) the PI-HYCOM simulation. The solid lines represent 95% significant level of Student's t test. Negative values represent upward motion for (a) and enhanced upward motion for (b)–(e).

motion is enhanced near the equator and the ITCZ is shifted northward with solar forcing, and they agree well with the observed vertical velocity and precipitation changes shown by van Loon et al. (2007). The vertical velocity responses of the PI-qflux and PI-HYCOM simulations (Figs. 6c,e) represent weak enhancement in the ascending motion near the equator and weakening of the descending motion in the descending branch. In general, the model simulations indicate that the ascending branch of the Hadley cell over the Pacific is enhanced by solar forcing in January, whereas the descending branch of the Hadley cell is weakened by solar forcing within the tropics but is expanded toward the midlatitudes. Solar signal in the coupled ocean model is generally smaller than in the mixed-layer model. Fully coupled ocean is able to mix heat down to the deep ocean, whereas the mixed layer is not, giving the dynamic ocean a much longer response time so that it will not have responded as completely to the forcing within a given simulation period (60 yr). The mixed layer will respond fully in a couple of decades, whereas the coupled model can take millennia.

The meridionally averaged vertical velocity in January over the equatorial band (from 10°S to 5°N) represents the Walker circulation along the equator in the Pacific and is characterized by the rising motion west of 150°W and sinking motion to the east (Fig. 7a). In addition to the Hadley circulation, the solar signals in the Walker circulation are shown in Figs. 7b–e from the model experiments through the differences of the meridionally averaged vertical velocity ω within the equatorial region between MAX and MIN. Over the region of the Pacific warm pool (150°E – 180°), the rising motion is enhanced in the MAX compared to the MIN in the PD-qflux, DF-PD-qflux, and PI-qflux simulations (Figs. 7b–d). Enhancement of the vertically ascending motion over the Pacific warm pool indicates the strengthening of the Walker circulation and is consistent with the increased specific humidity over this region, as shown in Figs. 4a–c. This result is also consistent with the enhancement of ascending motion near the equator as shown in Figs. 6b–d. The previous composition–climate modeling work of Shindell et al. (2006a) that includes a coupled dynamic ocean also showed the increase of the

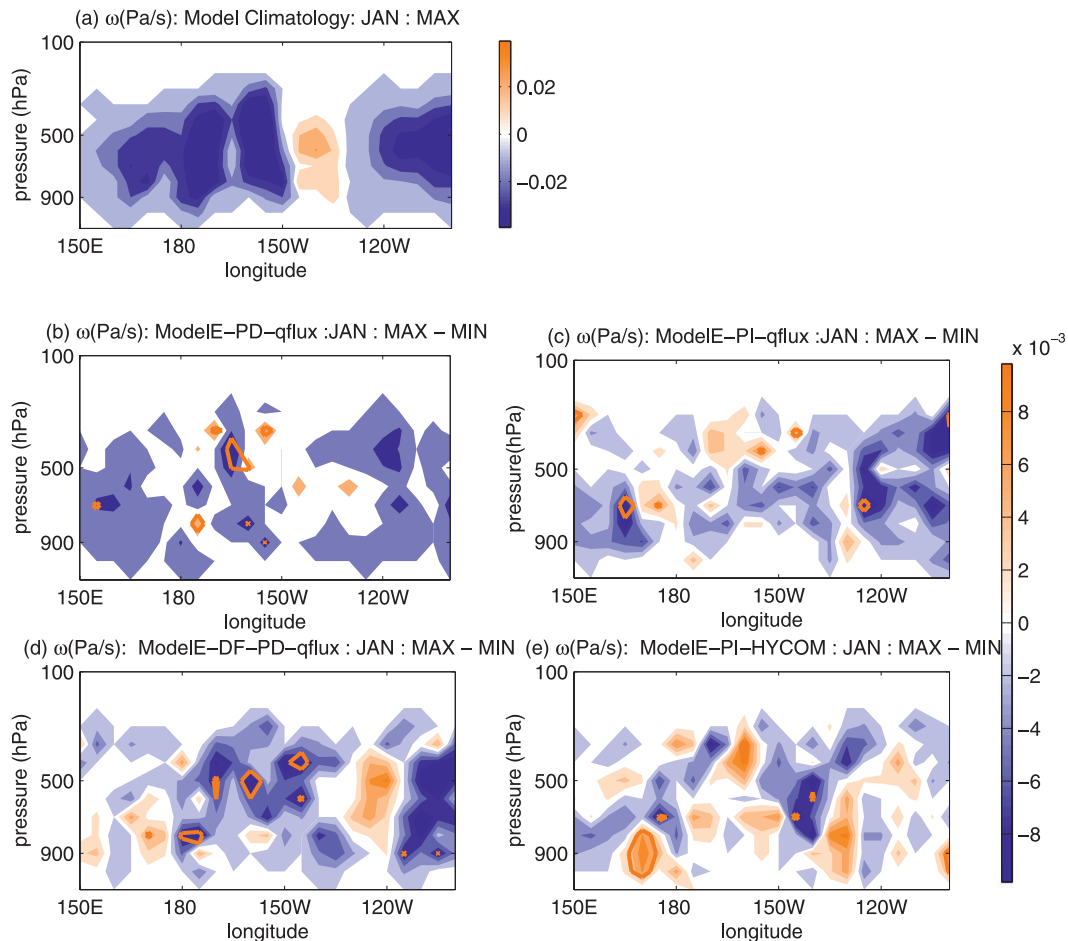


FIG. 7. Meridionally averaged vertical velocity ω over the tropical Pacific (10°S – 5°N) during the month of January in Pa s^{-1} for (a) the climatology from the model simulation, as well as the difference between MAX and MIN for (b) the PD-qflux simulation, (c) the PI-qflux simulation, (d) the DF-PD-qflux simulation, and (e) the PI-HYCOM simulation. The solid lines represent 95% significant level of Student's t test. Negative values represent upward motion for (a) and enhanced upward motion for (b)–(e).

annual mean precipitation in the Pacific warm pool region resulting from increased solar forcing.

b. Solar signal in tropical circulation in July

The differences of the zonally averaged vertical velocity in the PD-qflux simulation in July (Fig. 8b) show a weakening of the southern flank of the ascending branch between 5° and 10°S in MAX, which coincides with that of the observational result of van Loon et al. (2004). They show an intensification of the Hadley circulation in July and August, with increased vertical motion between 4° and 17°N and greater subsidence to the north and south of this area.

The DF-PD-qflux simulation (Fig. 8d) shows the similar solar signal with the PD-qflux simulation, but with the weakening of the northward part of the descending branch. Similar to the DF-PD-qflux simulation, the

vertical velocity responses of the PI-qflux simulation (Fig. 8c) represent weak enhancement in the ascending motion near the equator and substantial weakening of the descending branch. The responses in the PI-HYCOM simulation show weakening and a southward shift of the Hadley cell in the ascending branches. The intensified upwelling near the equator and the weakening of the upwelling in the northern part of the ascending branch in PI-qflux and PI-HYCOM simulations indicate a southward shift of the summer ITCZ. The Hadley circulation response patterns from the PI-qflux and PI-HYCOM runs with preindustrial composition appear to be consistent with the paleoclimate proxy records of the hydrological cycle from Hodell et al. (2001), Haug et al. (2001), and Lund et al. (2006).

The previous work of Shindell et al. (2006a) showed an annually averaged response of tropical zonal mean

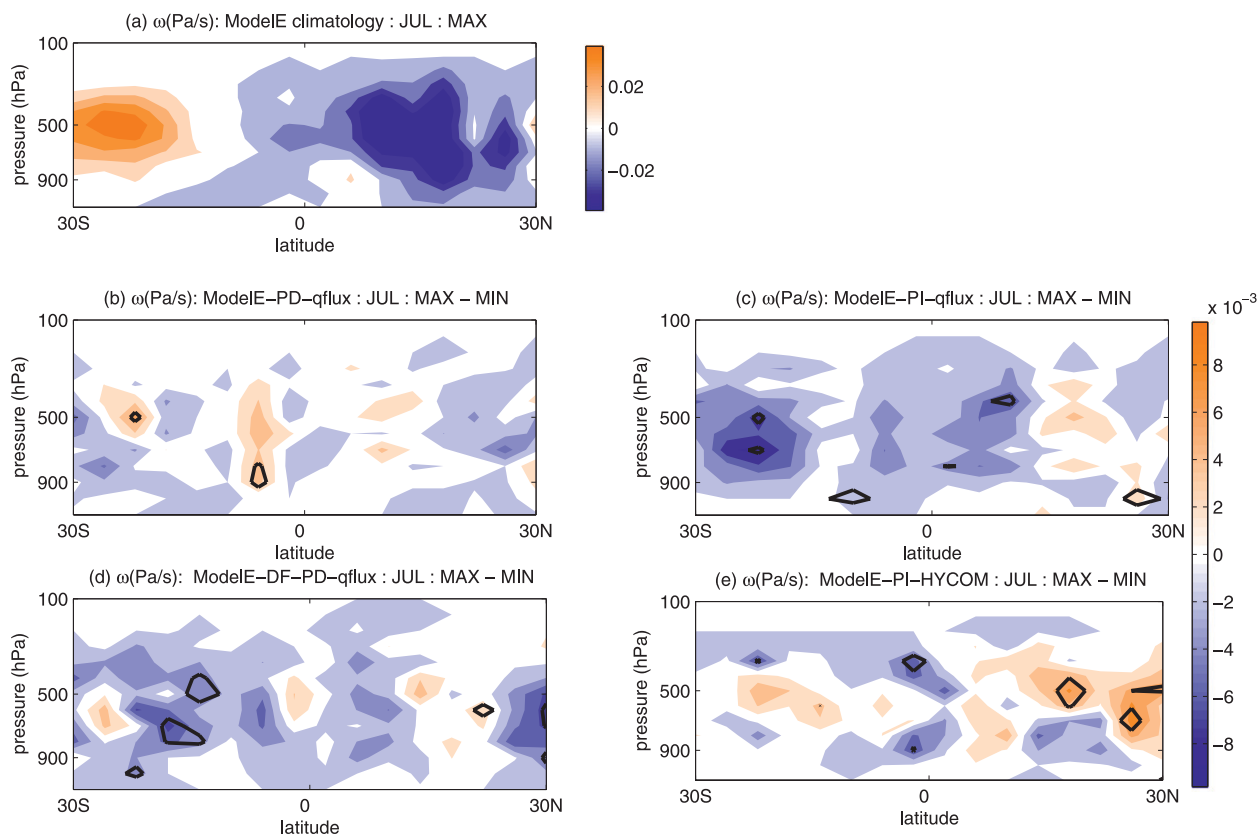


FIG. 8. As in Fig. 6, but for July.

circulation but not seasonal responses. Haigh et al. (2005) also showed weakening and expansion of the annually averaged Hadley cell. Hadley circulation can show a weakening on the annual average, whereas it strengthens during summer and/or winter. Seasonal responses of Hadley circulation are somewhat different from those of the annual mean responses of Shindell et al. (2006a), Matthes et al. (2006), and Haigh et al. (2005). They tended to find a weaker but broader Hadley cell. We also find broadening but not weakening of the seasonal Hadley cells. Rind et al. (2008) show an increase of upwelling and precipitation off the equator during July and August. Van Loon et al. (2004) also find an intensification of the Hadley circulation in July and August, with increased vertical motion between 5° and 17°N and greater subsidence to the north and south of this area.

The model responses in Walker circulation in July are illustrated in Fig. 9b–e by showing the differences in the vertical velocity between the MAX and MIN, from 150°E eastward to 90°W . In the PD-qflux simulation (Fig. 9b), there are stronger ascending regions in the equatorial western and the central Pacific but weaker ascending regions in the eastern Pacific in solar maxi-

mum. In all the simulations, the enhanced Walker cell with increased upward vertical motion in the western Pacific warm pool region is similar to that shown by van Loon et al. (2004) in the July–August averaged NCEP–NCAR vertical velocity. In the PI-qflux simulation (Fig. 9c), the upward motion in the eastern part of the Walker cell is significantly enhanced. The stronger upward motion (anomalous negative values) in this region during solar maximum is consistent with the increase of the integrated humidity (positive values) in Fig. 5b. Overall, the ascending branch of the Walker circulation shows strong uprising in response to solar forcing in the western Pacific, as is the case in January.

5. Conclusions

The response patterns of tropical humidity and vertical motion to solar forcing are season dependent and spatially heterogeneous. In the tropics, both the model and reanalysis consistently show that the specific humidity is significantly greater in the convective regions in solar maximum compared to solar minimum for January and July. The humidity response in the DF-PD-qflux simulation is enhanced by the doubled minimum forcing.

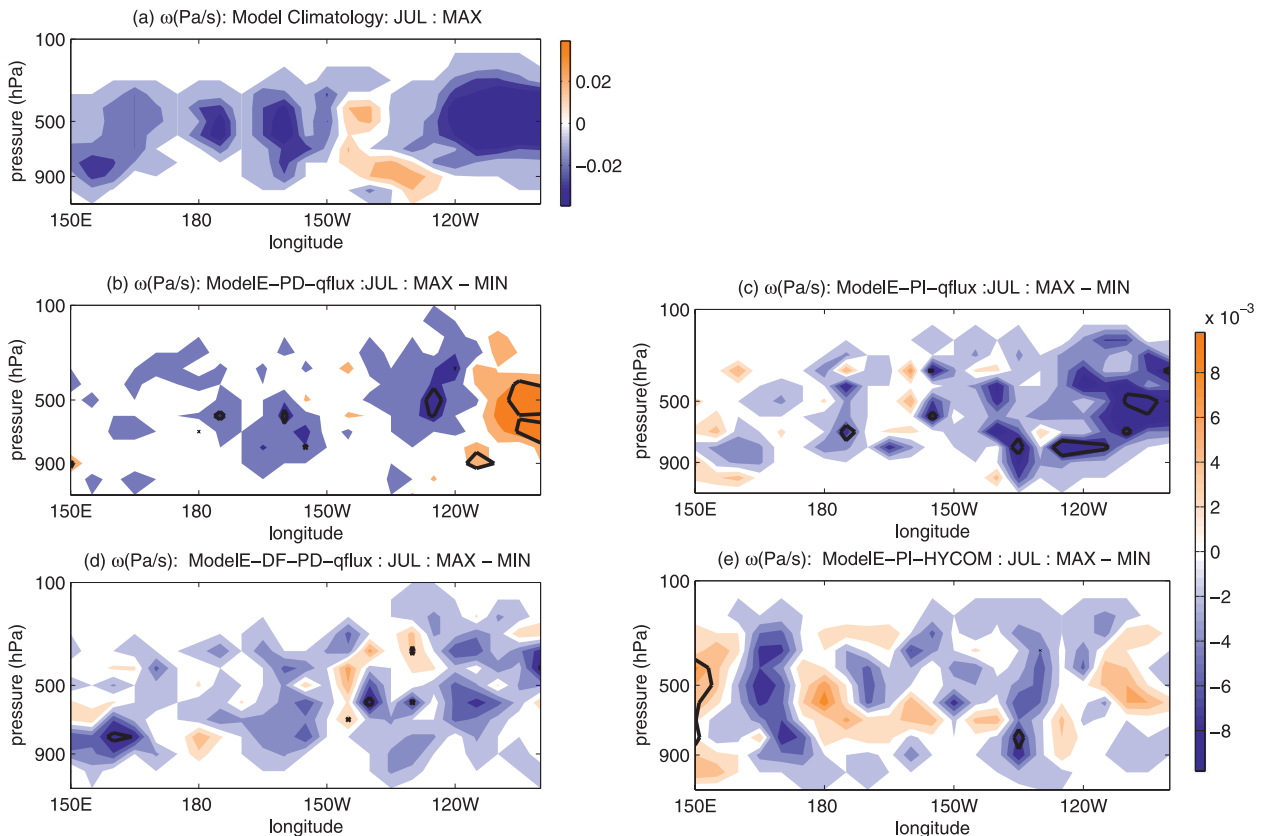


FIG. 9. As in Fig. 7, but for July.

In general, the latitude band of the significant positive humidity signal is broadened under the present-day (PD) greenhouse gas and aerosol conditions compared to the preindustrial (PI) conditions. The humidity responses indicate that tropical climate changes associated with the solar cycle include increased water vapor during solar maximum, which is similar to the responses expected from greenhouse gas increases (Cess et al. 1993). The column-integrated humidity in the model simulations increased with solar forcing in the tropical band over the Atlantic sector in both seasons, with different composition, different solar forcing, and different ocean models. Moreover, this positive signal extends from the Amazon area, past equatorial western Africa, to the western Pacific from Indonesia and to the west coast of Australia. This signal extends to the whole Pacific basin in the DF-PD-qflux run when the magnitude of the solar forcing is doubled.

In present-day conditions, the tropical circulation response to solar forcing is generally consistent with that derived from observations (van Loon et al. 2004, 2007; Kodera et al. 2007, 2008) in both solstice seasons. The responses of the zonally averaged vertical velocities in the PD-qflux and DF-PD-qflux simulations indicate that

the ascending branch of the Hadley cell is enhanced near the equator and the ITCZ is shifted northward in response to solar forcing during the boreal winter. The changes in vertical motion are not significantly increased by doubling the solar forcing. In the summer, the intensified upwelling near the equator and the weakening of the upwelling in the northern part of the ascending branch in the PI-qflux and PI-HYCOM simulations indicates a southward shift of the summer ITCZ. Response of the seasonal tropical circulation to the solar flux changes results in modulation of the strength and the position of the ascending and descending branches of Hadley circulation, which are related to regional seasonal monsoon circulations. When preindustrial conditions are imposed, the Hadley circulation response patterns from the model agree with proxy records, which show correlation between regional drought and solar variability.

Enhancement of the meridionally averaged vertical velocity over the western Pacific indicates strengthening of the Walker circulation in response to solar forcing in both solstice seasons. Both in model and observation, the changes in dynamic properties associated with solar variability are weaker than those associated with anthropogenic forcing or with ENSO events, and they are

often not statistically significant in most of the tropical troposphere (Lee and Hameed 2007; Lee et al. 2008; Rind et al. 2008). However, by conducting a set of simulations with different greenhouse gas conditions, different amplitudes of solar forcing, and different ocean models, we can conclude with a sufficiently consistent pattern that indicates the seasonal movement of the Hadley circulation and strengthening of the Walker circulation.

The previous work of Shindell et al. (2006a) showed an annually averaged response of tropical zonal mean circulation but not seasonal responses. Haigh et al. (2005) also showed weakening and expansion of the annually averaged Hadley cell. Hadley circulation can show a weakening in the annual average, whereas it strengthens during summer and/or winter. Seasonal responses of Hadley circulation are somewhat different from those of annual mean responses of Shindell et al. (2006a) and Haigh et al. (2005). They tended to find a weaker but broader Hadley cell. We also find broadening, but not weakening of the seasonal Hadley cells. With a different version of the GISS model, Rind et al. (2008) also show an increase of upwelling and precipitation off the equator during July and August. Van Loon et al. (2004) also find an intensification of the Hadley circulation in July and August, with increased vertical motion between 4° and 17°N, and greater subsidence to the north and south of this area.

The statistical significance of the solar signal in the model's vertical velocities is not consistent with the different atmospheric composition, solar forcing, and ocean model for most regions of the atmosphere. This includes the possibility that the tropical circulation response to solar variability depends strongly on the greenhouse gas conditions, amplitude of solar forcing, and the coupled ocean model. Hence, further work is clearly required to establish if the model's sensitivity to solar forcing is realistic and to better characterize the causes of the apparent dependence of the response to the background composition, the oceanic response, and the amplitude of the solar forcing. It is also difficult to isolate the solar UV effect from that of TSI, because to date the modeling works force the entire spectrum of solar variability in one simulation. It is required to simulate the UV forcing and IR forcing separately, besides the TSI, so that the response from the individual bands and their interactions can be clearly identified. Spectral solar irradiance (SSI) is available from Spectral Irradiance Monitor (SIM) as part of National Aeronautics and Space Administration (NASA) Earth Observing System (EOS) Solar Radiation and Climate Experiment (SORCE) mission since August 2003 to the present (Harder et al. 2009). Newly observed SSI measurements

also can provide more reliable input of solar irradiance to GCM simulations.

Acknowledgments. This work was supported by the NASA Living with a Star Program and Atmospheric Chemistry Modeling and Analysis Program. We thank Greg Faluvegi for running the GISS GCM and organizing the model outputs, and we thank Christy Field for performing the doubled forcing simulation. We also thank Minghua Zhang for providing the NCAR Community Climate Model (CCM2) radiation parameterization code and Hua Song, David Black, Dong L. Wu, and Marat Khairoutdinov for useful discussions. We also thank two anonymous reviewers for suggestions and comments that have led to significant improvements of the paper.

REFERENCES

- Angell, J. K., and J. Korshover, 1981: Comparison between sea surface temperature in the equatorial eastern Pacific and United States surface temperature. *J. Appl. Meteor.*, **20**, 1105–1110.
- Berger, A. L., 1978: Long-term variations of caloric insolation resulting from the earth's orbital elements. *Quat. Res.*, **9**, 139–167.
- Black, D. E., R. C. Thunell, L. C. Peterson, A. Kaplan, and E. J. Tappa, 2004: A 2000-year record of tropical North Atlantic hydrographic variability. *Paleoceanography*, **19**, PA2022, doi:10.1029/2003PA000982.
- Bony, S., and Coauthors, 2006: How well do we understand and evaluate climate change feedback processes? *J. Climate*, **19**, 3445–3482.
- Carlson, A. E., A. N. LeGrande, D. W. Oppo, R. E. Came, G. A. Schmidt, F. S. Anslow, J. M. Licciardi, and E. A. Obbink, 2008: Rapid early Holocene deglaciation of the Laurentide ice sheet. *Nat. Geosci.*, **1**, 620–624, doi:10.1038/ngeo285.
- Cess, R. D., and Coauthors, 1993: Uncertainties in carbon dioxide radiative forcing in atmospheric general circulation models. *Science*, **262**, 1252–1255.
- Chen, Y., A. D. Del Genio, and J. Chen, 2007: The tropical atmospheric El Niño signal in satellite precipitation data and a global climate model. *J. Climate*, **20**, 3580–3601.
- Fleitmann, D., S. J. Burns, M. Mudelsee, U. Neff, J. Kramers, A. Mangini, and A. Matter, 2003: Holocene forcing of the Indian monsoon recorded in a stalagmite from southern Oman. *Science*, **300**, 1737–1739.
- Gleisner, H., and P. Thejll, 2003: Patterns of tropospheric response to solar variability. *Geophys. Res. Lett.*, **30**, 1711–1714.
- Hack, J. J., B. A. Boville, B. P. Briegleb, J. T. Kiehl, P. J. Rasch, and D. L. Williamson, 1993: Description of the NCAR Community Climate Model (CCM2). NCAR Tech. Note NCAR/TN-382+STR, 108 pp.
- Haigh, J., M. Blackburn, and R. Day, 2005: The response of tropospheric circulation to perturbations in lower-stratospheric temperature. *J. Climate*, **18**, 3672–3685.
- Harder, J. W., J. M. Fontenla, P. Pilewskie, E. C. Richard, and T. N. Woods, 2009: Trends in solar spectral irradiance variability in the visible and infrared. *Geophys. Res. Lett.*, **36**, L07801, doi:10.1029/2008GL036797.

- Haug, G. H., K. A. Hughen, D. M. Sigman, L. C. Peterson, and U. Röhl, 2001: Southward migration of the intertropical convergence zone through the Holocene. *Science*, **293**, 1304–1308.
- , D. Gunther, L. C. Peterson, D. M. Sigman, K. A. Hughen, and B. Aeschlimann, 2003: Climate and the collapse of Maya civilization. *Science*, **299**, 1731–1735.
- Held, I. M., and B. J. Soden, 2006: Robust responses of the hydrological cycle to global warming. *J. Climate*, **19**, 5686–5699.
- Hodell, D. A., M. Brenner, J. H. Curtis, and T. Guilderson, 2001: Solar forcing of drought frequency in the Maya lowlands. *Science*, **292**, 1367–1370.
- John, V. O., and B. J. Soden, 2007: Temperature and humidity biases in global climate models and their impact on climate feedbacks. *Geophys. Res. Lett.*, **34**, L18704, doi:10.1029/2007GL030429.
- Kalnay, E., and Coauthors, 1996: the NCEP/NCAR 40-Year Reanalysis Project. *Bull. Amer. Meteor. Soc.*, **77**, 437–471.
- Kodera, K., 2004: Solar influence on the Indian Ocean Monsoon through dynamical processes. *Geophys. Res. Lett.*, **31**, L24209, doi:10.1029/2004GL020928.
- , 2007: The role of dynamics in solar forcing. *Space Sci. Rev.*, **125**, 319–330, doi:10.1007/s11214-006-9066-1.
- , and K. Shibata, 2006: Solar influence on the tropical stratosphere and troposphere in the northern summer. *Geophys. Res. Lett.*, **33**, L19704, doi:10.1029/2006GL026659.
- , K. Coughlin, and O. Arakawa, 2007: Possible modulation of the connection between the Pacific and Indian Ocean variability by the solar cycle. *Geophys. Res. Lett.*, **34**, L03710, doi:10.1029/2006GL027827.
- , M. E. Hori, S. Yukimoto, and M. Sigmond, 2008: Solar modulation of the northern hemisphere winter trends and its implications with increasing CO₂. *Geophys. Res. Lett.*, **35**, L03704, doi:10.1029/2007GL031958.
- Lean, J., 2000: Evolution of the Sun's spectral irradiance since the Maunder Minimum. *Geophys. Res. Lett.*, **27**, 2425–2428.
- Lee, J. N., and S. Hameed, 2007: The Northern Hemisphere annular mode in summer: Its physical significance and its relation to solar activity variations. *J. Geophys. Res.*, **112**, D15111, doi:10.1029/2007JD008394.
- , —, and D. T. Shindell, 2008: The northern annular mode in summer and its relation to solar activity variations in the GISS ModelE. *J. Atmos. Terr. Phys.*, **70**, 730–741, doi:10.1016/j.jastp.2007.10.012.
- Li, D., and K. P. Shine, 1995: A 4-dimensional ozone climatology for UGAMP models. UGAMP Internal Rep. 35.
- Lindzen, R. S., M.-D. Chou, and A. Y. Hou, 2001: Does the earth have an adaptive infrared iris? *Bull. Amer. Meteor. Soc.*, **82**, 417–432.
- Lund, D. C., J. Lynch-Stieglitz, and W. B. Curry, 2006: Gulf Stream density structure and transport during the past millennium. *Nature*, **444**, 601–604.
- Matthes, K., Y. Kuroda, K. Kodera, and U. Langematz, 2006: Transfer of the solar signal from the stratosphere to the troposphere: Northern winter. *J. Geophys. Res.*, **111**, D06108, doi:10.1029/2005JD006283.
- Mayle, F. E., R. Burbridge, and T. J. Killeen, 2000: Millennial-scale dynamics of southern Amazonian rain forests. *Science*, **290**, 2291–2294.
- Meehl, G. A., and A. Hu, 2006: Megadroughts in the Indian monsoon region and southwest North America and a mechanism for associated multidecadal Pacific sea surface temperature anomalies. *J. Climate*, **19**, 1605–1623.
- , W. M. Washington, T. M. L. Wigley, J. M. Arblaster, and A. Dai, 2003: Solar and greenhouse gas forcing and climate response in the twentieth century. *J. Climate*, **16**, 426–444.
- Otto-Bliesner, B. L., E. C. Brady, G. Clauzet, R. Tomas, S. Levis, and Z. Kothavala, 2006: Last Glacial Maximum and Holocene climate in CCSM3. *J. Climate*, **19**, 2526–2544.
- Pierrehumbert, R. T., 2001: Basic principles of climate. *Proceedings of the 2001 Program in Geophysical Fluid Dynamics: Conceptual Models of the Climate*, Woods Hole Oceanographic Institution, 88–97. [Available online at http://www.whoi.edu/cms/files/lect_07_2001_21421.pdf.]
- , H. Brogniez, and R. Roca, 2005: On the relative humidity of the atmosphere. *The Global Circulation of the Atmosphere*, T. Schneider and A. Sobel, Eds., Princeton University Press, 143–185.
- Rind, D., J. Perlwitz, P. Lonergan, and J. Lerner, 2005: AO/NAO response to climate change: 2. Relative importance of low- and high-latitude temperature changes. *J. Geophys. Res.*, **110**, D12108, doi:10.1029/2004JD005686.
- , J. Lean, J. Lerner, P. Lonergan, and A. Leboissier, 2008: Exploring the stratospheric/tropospheric response to solar forcing. *J. Geophys. Res.*, **113**, D24103, doi:10.1029/2008JD010114.
- Ruzmaikin, A., J. Feynman, and Y. L. Yung, 2006: Is solar variability reflected in the Nile River? *J. Geophys. Res.*, **111**, D21114, doi:10.1029/2006JD007462.
- Salby, M., and P. Callaghan, 2005: Interaction between the Brewer–Dobson circulation and the Hadley circulation. *J. Climate*, **18**, 4303–4316.
- Schmidt, G. A., D. T. Shindell, R. L. Miller, M. E. Mann, and D. Rind, 2004: General circulation modelling of Holocene climate variability. *Quat. Sci. Rev.*, **23**, 2167–2181, doi:10.1016/j.quascirev.2004.08.005.
- , and Coauthors, 2006: Present-day atmospheric simulations using GISS ModelE: Comparison to in situ, satellite, and reanalysis data. *J. Climate*, **19**, 153–192.
- Schmidt, H., and Coauthors, 2006: The HAMMONIA chemistry climate model: Sensitivity of the mesopause region to the 11-year solar cycle and CO₂ doubling. *J. Climate*, **19**, 3903–3931.
- Shindell, D. T., G. A. Schmidt, M. E. Mann, D. Rind, and A. Waple, 2001: Solar forcing of regional climate change during the Maunder Minimum. *Science*, **294**, 2149–2152, doi:10.1126/science.1064363.
- , G. Faluvegi, R. L. Miller, G. A. Schmidt, J. E. Hansen, and S. Sun, 2006a: Solar and anthropogenic forcing of tropical hydrology. *Geophys. Res. Lett.*, **33**, L24706, doi:10.1029/2006GL027468.
- , —, N. Unger, E. Aguilar, G. A. Schmidt, D. Koch, S. E. Bauer, and R. L. Miller, 2006b: Simulations of preindustrial, present-day, and 2100 conditions in the NASA GISS composition and climate model G-PUCCINI. *Atmos. Chem. Phys.*, **6**, 4427–4459.
- Soukharev, B. E., and L. L. Hood, 2006: Solar cycle variation of stratospheric ozone: Multiple regression analysis of long-term satellite data sets and comparisons with models. *J. Geophys. Res.*, **111**, D20314, doi:10.1029/2006JD007107.
- Sun, D.-Z., and I. M. Held, 1996: A comparison of modeled and observed relationships between interannual variations of water vapor and temperature. *J. Climate*, **9**, 665–675.
- Sun, S., and R. Bleck, 2006: Multi-century simulations with the coupled GISS-HYCOM climate model: Control experiments. *Climate Dyn.*, **26**, 407–428.
- van Loon, H., and K. Labitzke, 1994: The 10–12-year atmospheric oscillation. *Meteor. Z.*, **3**, 259–266.

- , G. A. Meehl, and J. M. Arblaster, 2004: A decadal solar effect in the tropics in July–August. *J. Atmos. Sol.-Terr. Phys.*, **66**, 1767–1778, doi:10.1016/j.jastp.2004.06.003.
- , ———, and D. J. Shea, 2007: Coupled air-sea response to solar forcing in the Pacific region during northern winter. *J. Geophys. Res.*, **112**, doi:10.1029/2006JD007378.
- Wang, X., A. S. Auler, R. L. Edwards, H. Cheng, P. S. Cristalli, P. L. Smart, D. A. Richards, and C.-C. Shen, 2004: Wet periods in northeastern Brazil over the past 210 kyr linked to distant climate anomalies. *Nature*, **432**, 740–743.
- Wang, Y.-M., J. L. Lean, and N. R. Sheeley Jr., 2005: Modeling the sun's magnetic field and irradiance since 1713. *Astrophys. J.*, **625**, 522–538.
- White, W. B., M. D. Dettinger, and D. R. Cayan, 2003: Sources of global warming of the upper ocean on decadal period scales. *J. Geophys. Res.*, **108**, 3248, doi:10.1029/2002JC001396.
- Zhang, T., K. Stamnes, and S. A. Bowling, 2001: Impact of the atmospheric thickness on the atmospheric downwelling long-wave radiation and snowmelt under clear-sky conditions in the arctic and subarctic. *J. Climate*, **14**, 920–939.